Sigma J Eng & Nat Sci 38 (2), 2020, 907-926

Sigma Journal of Engineering and Natural Sciences
Sigma Mühendislik ve Fen Bilimleri Dergisi

Research Article

EVALUATION OF THE EFFECTS OF LAND COVER CHANGES AND URBANIZATION ON LAND SURFACE TEMPERATURE: A REMOTE SENSING STUDY OF SUB-WATERSHED OF OUED FEKAN, NORTHWEST ALGERIA

Mohammed CHRAIR*[1], A. KHALDI[2], M. A. HAMADOUCHE[3], A. HAMIMED[4], Flavie CERNESSON[5], Mehmet ALKAN[6]

[1]*Laboratory of Research on Biological Systems and Geomatics, Faculty of Science of Nature and Life, University Mustapha Stambouli of Mascara, ALGERIA;* ORCID: 0000-0003-4422-9950
[2]*Laboratory of Research on Biological Systems and Geomatics, Faculty of Science of Nature and Life, University Mustapha Stambouli of Mascara, ALGERIA;* ORCID: 0000-0002-4068-0878
[3]*Laboratory of Research on Geomatics, Ecology and Environment, University Mustapha Stambouli of Mascara, ALGERIA;* ORCID: 0000-0001-6009-2726
[4]*Laboratory of Research on Biological Systems and Geomatics, Faculty of Science of Nature and Life, University Mustapha Stambouli of Mascara, ALGERIA;* ORCID: 0000-0002-3141-6813
[5]*AgroParisTech, UMR TETIS - Territoires, Environnement, Télédétection et Information Spatiale, 500 Rue Jean François Breton, 34000 Montpellier, FRANCE;* ORCID: 0000-0001-9586-065X
[6]*Yıldız Technical University, ISTANBUL;* ORCID: 0000-0002-7542-5455

Received: 15.11.2019 Revised: 10.03.2020 Accepted: 06.04.2020

ABSTRACT

Urban growth is a worldwide phenomenon. The rate of urbanisation in developing countries such as Algeria is speedy. Sub-watershed of Oued Fekan is included in the large watershed of Macta which is located in north-western Algeria and is one of the most important sites of this country characterized by an abundant amount of biodiversity as well as a highly productive ecosystem. The valuable landscape undergoes a radical change in the form of a sub-watershed recently due to anthropogenic change on land use and land cover. The exponential increase in population and human activities are increasing the demand for land and soil resources for agriculture, urban and industrial uses. Anthropogenic factors, especially urban sprawl, have a significant role in controlling the temperature change.

In this paper, four Landsat-8 OLI/TIRS images of 2018 have been used from different seasons to estimate land surface temperature (LST), Normalized Difference Built-up Index (NDBI) and Normalized Difference Vegetation Index (NDVI) in order to study the phenomenon of difference distribution temperature in urban with the surrounding rural areas. Analysis based on linear regression was used to generate relationships between LST with NDVI and NDBI. Our analysis indicates that for the four seasons, a strong linear relationship between NDBI and LST was marked compared with the relationship between NDVI and LST, which was less intense and varied by seasons. We suggest that NDBI is a visible indicator for studying surface Urban Heat Island phenomenon (UHI). Useful information that occurs as a consequence of land-use changes and urbanization are then provided for understanding the local climate and environmental changes of our study area.

Keywords: Land surface temperature, urban heat Island, climate change, urbanization, landsat, Algeria.

* Corresponding Author: e-mail: chrair29mohamed@gmail.com, tel: + 213 45 71 66 89

1. INTRODUCTION

Over the last three decades and all over the world, remote sensing data were and steeled the essential components of many applications. One of these essential applications areas is to determine and analyse changes in land use, land cover and urbanization. In Algeria, decision-makers have provided farmers and landowners the opportunity to lease land for additional cultivation (individual/collective agricultural holding), while limiting urban growth and promoting local product ion. The program supported by superior authorities, encourages the return to agricultural areas which were deserted in the past, has allowed multiplying the number of new farms constructions. The growth of urban areas and industrial intensification, has contributed to a reduction in valuable agricultural lands and various environmental impacts, such as increased surface temperature. This phenomenon of conversion of vegetated land to impervious lands, including settlements was the reason for the conversion of pixels of cooling to a higher temperature surface [1]. Land surface temperature (LST) is crucial parameters in the physics of land surface processes at local to global scales. Availability of spatial data and the particular interest of the scientific community by developing retrieving algorithm and methodologies to measure LST from space shows the exponential importance of this index in different fields of research. Since its retrieval problem is ill-posed, retrieving LST remains a challenging task [2]. Air temperature between an urban and a rural site is different. Towns and cities are warmer at night compared to rural areas because of the absorption of the Sun's radiation in urban concrete and buildings. This phenomenon is called Urban Heat Island (UHI) [3]. According to Mascara census office, the population of our study area is exponentially increasing. The growth of urban areas and industrial intensification contributes to an augmentation in air temperatures, such as climatic change and global warming potential. Thus it has become a topical, and one of the significant issues for environmental researches. The surface heat flux controls LST and urbanization lead to exacerbating this phenomenon, the effect of UHI is caused by the spatial distribution of LST [4-5].

Consequently, obtaining LST is critical for the analysis of UHI [6]. Remote sensing technology keeps playing the leading role in the understanding of our environment. It has evolved into an integral research tool for the natural sciences with the increasing of its imagery resolution. It has become an essential approach to UHI research. The traditional method for analyzing UHI is based on LST data measured at local observation points. With the appearance of high-resolution earth monitoring satellites, it became possible and more practical to measure LST using remote sensing technology and to obtain also an additional UHI primary data [6-7]. The traditional method of meteorological observation may not be sufficient to cover the entire region understudy because of uneven distribution and the limited conditions of data collected from local meteorological observations points. New techniques of remote sensing have the favour of the high spatial resolution, which enables large-scale research of UHI [6]. Several pieces of research have been carried out on the use of remote sensing tools and GIS for multiple subjects such as monitoring biodiversity, creating LST and change detection maps.

Previous works are mentioned here: Several studies revealed UHI spatial patterns counting the relationship between UHI and land use/cover types [8-9-10]. Many authors have worked on several remote sensing datasets used in UHI studies and have emphasized different cognitive issues. Balling and Brazel used Advanced Very High-Resolution Radiometer AVHRR thermal bands for estimating LST over Phoenix in Arizona and obtained reliable results of LST variations across the metropolitan area [11]. Therefore, Sobrino developed a split-window equation after simulations of satellite measurements of LST using the atmospheric transmittance-radiance model LOWTRAN-7 for NOAA-11 AVHRR Channels 4 and 5 [12]. Streutker showed that satellite radiance data could be used to characterize both the magnitude and spatial extent of an urban heat island (UHI) after his work in Houston, Texas. One year after, in the same study area, he proved the growth of the surface temperature using the split-window infrared channels of the AVHRR

[13-14]. Weng focused on the rela tionship between LST and vegetation abundance for UHI studies in the city of Indianapolis, USA. LST was derived from the corrected Landsat ETM+ TIR band in this research [15]. Recently, based only on Landsat imagery, Fu and Weng devised an algorithm to generate spatially and temporally sustained LSTs at Landsat spatial resolution to overcome limitations of Landsat TIR sensor, which do not allow generating LSTs at any desired date with consistent accuracy and corrections [16]. Hu and Brunsell studied the impact of temporal aggregation on LST and UHI from 2000 to 2010. They quantified this impact focusing on Houston, Texas and its surroundings using MODIS LST products, using the generalized split-window LST algorithm [17]. In our study area, studies were conducted mainly for monitoring evapotranspiration and surface energy fluxes estimation; Nehal used Thermal (band 6) of Landsat-7 ETM+ Image to estimate LST. The present study aims to retrieve LST from Landsat 8 OLI-TIRS Imagery, using Mono-window algorithm, and to compare NDBI and NDVI as indicators of UHI by looking for the best correlation between each one of the two indices and the LST [18].

A recent study compares NDBI and NDVI as indicators of SUHI effects using MODIS imagery, the result suggests NDBI as an accurate indicator of SUHI effects and can be used as a complementary metric to the traditionally applied NDVI for analyzing LST quantitatively during the year for SUHI studies [19]. Different scholars in different time periods attempted to draw a correlation between LST in UHIs and some LU/LC indices applied in several countries. The majority used thermal remote sensing data to estimate the indices [20-21-22-23-24]. In the aim to classify different LU/LC types using NDVI and NDBI threshold values, LST with both indices were estimated using Landsat 8 data, this analytical study was applied to investigate the UHI intensity effect for Florence and Naples cities in Italy, and to interpret the dynamic relationship between LST with NDVI and NDBI [25].

2. MATERIAL AND METHODS

2.1. Study area

The study area is located in Mascara city, mainly, in sub-watershed of Oued Fekan(fig.1.b), located in north-western of Algeria between latitude 35° 7'N to 35° 31' N and longitude 0° 25' W to 0° 4.143' E, thereby covering a total geographical area of approximately 1195 km². It includes the Ghriss plain which covers an agricultural area of more than 72000 hectares. It is limited from the north by the Beni-Chougrane Mountains, from the south by the Saida Mountains, from the west by Bouhanifia Mountains and in the east, we find the trays of Tighennif.

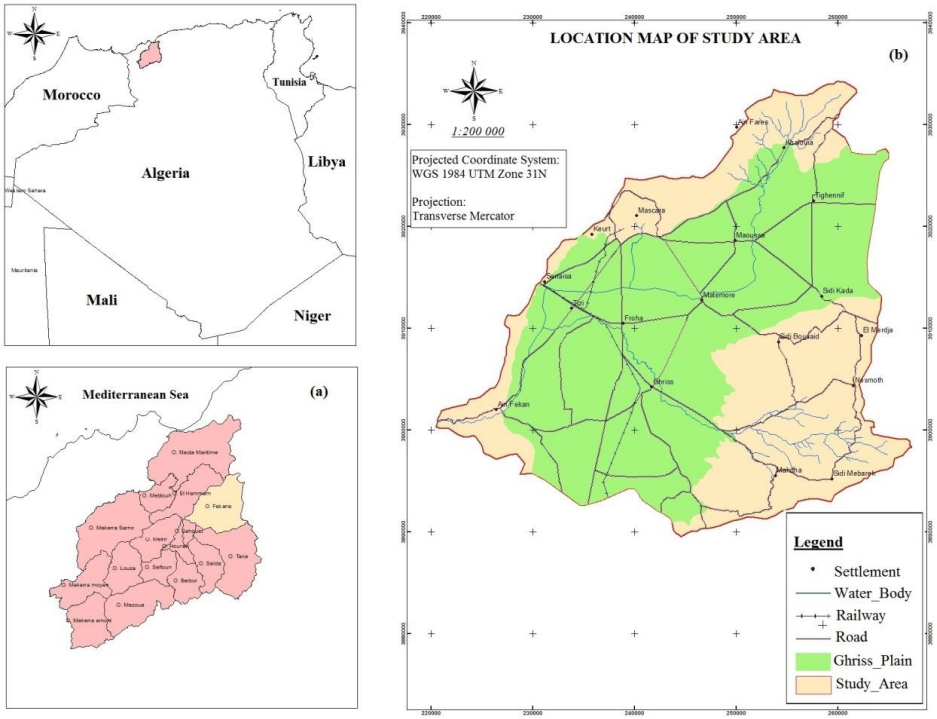

Figure 1. Location map of study area (a) Sub-watersheds of the Macta, (b) sub-watershed of Oued Fekan.

2.1.1. Topography

The plain corresponds to a flat stretch with an average altitude of 450 m, overhanging by high edge ridges that exceed the 1000 m of altitude in the south (Nesmoth Mountain). Non-permanent watercourses drain this topographic catchment area which is upstream in the mountains of Beni-Chougrane and Nesmoth, while its downstream is located in the western part. The western part is the outlet which feeds the Bouhanifia dam.

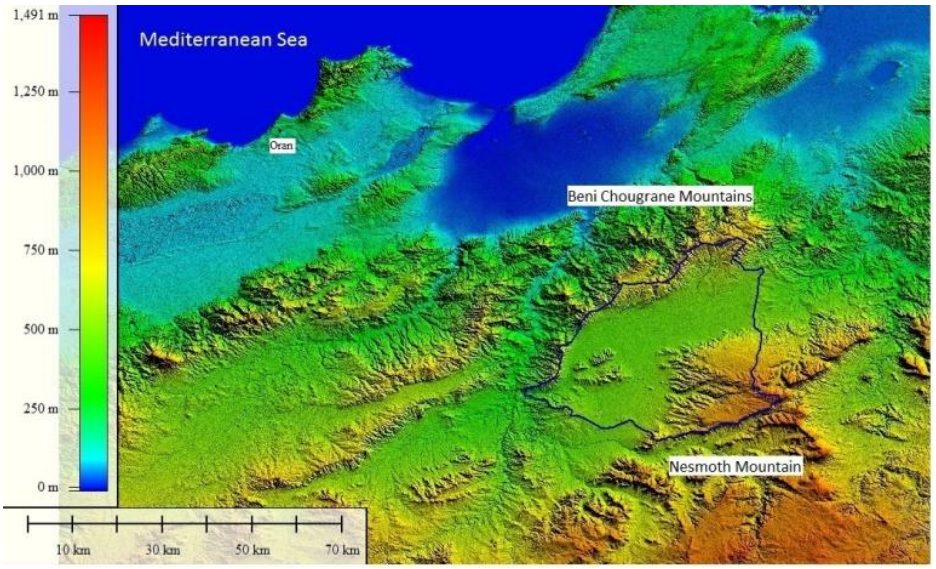

Figure 2. Digital Elevation Model of Oued Fekan.

2.1.2. Climatic and rainfall context

This region is characterized by a semi-arid climate where the annual average of precipitations is around 313 mm/year for the period of 1976-2001 [26]. For the same period, the actual evapotranspiration was estimated at 289 mm/year while the average annual temperature is 16.5 °C. The accumulated rainfall between December and February corresponds on average to 37% of the total annual rainfall. The spring and autumn rains correspond respectively to 30% and 28% of this total, while the summer rains, which are stormy and torrential, represent only 5% of the total. The area has no significant spatial rainfall variability although the landforms are more watered than the central plain. Very high temperatures are measured during the period from June to August with maximum values exceeding 40 °C during the day. It favours the evaporation of the waters of the superficial aquifer. The wadis of the plain have non-perennial flows with very low or null annual average flows.

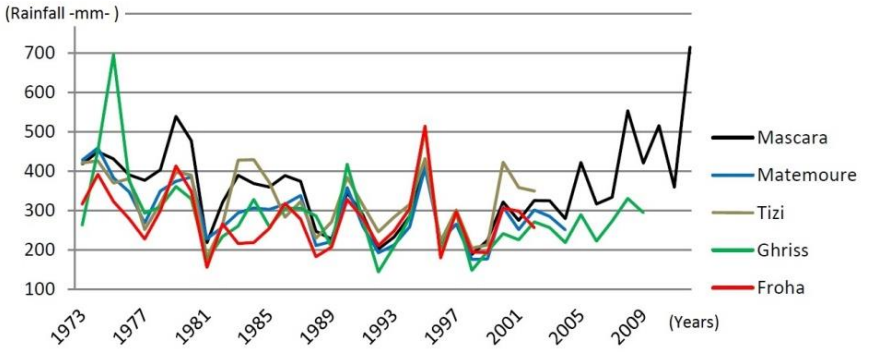

Figure 3. Evolution of rainfall in Mascara, Matemoure, Tizi, Ghriss and Froha meteorological station.

2.1.3. Soil representation

The study of pedology is essential to understand the nature and types of the soils that exist in Oued Fekan region. This part has been permanently taken from works made at the ANRH (National Agency of Hydraulic Resources) level where the plain has been the subject of many soil surveys. Lands which outcropping the plain are from the sedimentary formation with variable texture, composed predominately of recent and older alluvium. Generally, soils are of calcimagnesic type, but occasionally we meet isohumic and poorly evolved soils [18]. All these types of soil in the study area are favourable to the infiltration of precipitation water for recharging plio-quaternary groundwater and represent the nourishing ground, naturally fertile. Its significant agricultural potential characterizes the plain since more than 90% of its total area is currently used for agricultural activity.

2.2. Data sources

Our study area is fully included in the Landsat 8, Path/Row 197/36. As shown on the table 1, the images used in this analysis were acquired in 2018, respectively in February, May, August and November so that it covers four different seasons. Images of Landsat 8 OLI-TIRS (Operational Land Imager Thermal Infrared Sensor) are downloaded from the Earth Explorer US Geological Survey image database (Landsat Imagery Archive).

Table 1. Specification of the used satellites images.

Satellite	Sensor	Path/Row	Year	Month	Time	Resolution (m)	Wavelength µm
Landsat 8	OLI (Operational Land Imager) and TIRS (Thermal Infrared Sensor)	197/36	2018	February May August November	10:32	30 (For TIRS bands resolution is 100 m) (For band 8 resolution is 15 m)	Band 1: 0.435-0.451 Band 2: 0.452–0.512 Band 3: 0.533–0.590 Band 4: 0.636–0.673 Band 5: 0.851–0.879 Band 6: 1.566–1.651 Band 7: 2.107–2.294 Band 8: 0.50–0.68 Band 9: 1.363–1.384 Band 10: 10.60–11.19 (Thermal band) Band 11: 11.50–12.51 (Thermal band)

2.2.1. Preprocessing of OLI Data

The USGS EROS Center provides standard Landsat 8 data products. It consists of quantized and calibrated scaled Digital Numbers (DN) representing multispectral image data acquired by both the Thermal Infrared Sensor (TIRS) and Operational Land Imager (OLI). The products are delivered in 16-bits; we rescaled them to the Top of Atmosphere (TOA) radiance using radiometric rescaling coefficients provided in the product metadata file (MTL file).

$$L_\lambda = M_L Q_{cal} + A_L \quad (1)$$

Where $L\lambda$ is TOA spectral radiance (Watts/ (m2 * srad * µm)), M_L is Band-specific multiplicative rescaling factor from the metadata (RADIANCE_MULT_BAND_x, where x is the band number), AL is Band-specific additive rescaling factor from the metadata

(RADIANCE_ADD_BAND_x, where x is the band number), Q_{cal} is Quantized and calibrated standard product pixel values (DN).

The spectral radiance in the optical range is converted into reflectance after correction for atmospheric effects using commercially-available MODTRAN Software radiative transfer code [27]. These reflectances are subsequently exploited to calculate the normalized difference vegetation index (NDVI) and the normalized difference built-up index (NDBI).NDVI optimize contrasts between the infrared and the visible bands. This index makes it possible to visualize, on a single channel, the dynamic responses related to the density of vegetative cover. NDVI is included between -1 and +1.When the area corresponding to the soil has a strong chlorophyllin activity; it marks a high value [28]. NDVI is then calculated as the combination between near infrared and red band:

$$NDVI = \frac{(R_{NIR} - R_{RED})}{(R_{NIR} + R_{RED})} \quad (2)$$

NDBI based on the analysis of the unique spectral responses of built-up areas in seven Landsat TM bands. The original NDBI approach developed by Zha is implemented based on Landsat OLI bands covering NIR and SWIR wavelength [29], using the following equations:

$$NDBI = \frac{(R_{SWIR} - R_{NIR})}{(R_{SWIR} + R_{NIR})} \quad (3)$$

2.2.2. Pre-processing of TIRS Data

The following relationship express the spectral space-reaching radiance ($L^{\uparrow}sat(\lambda)$) measured by the sensor in the thermal infrared:

$$L^{\uparrow}sat(\lambda) = \left[\varepsilon_0 L_\lambda(T_0) + (1-\varepsilon_0) L^{\downarrow}atm(\lambda)\right] * \tau_\lambda + L^{\uparrow}atm(\lambda)] \quad (4)$$

Where:

$L_\lambda(T_0)$ is the radiance of a blackbody target of kinetic temperature T_0.

τ_λ is atmospheric transmission.

$L^{\downarrow}atm(\lambda)$ is the down welling or sky radiance.

$L^{\uparrow}atm(\lambda)$ is the upwelling or atmospheric path radiance.

Both atmospheric parameters (τ_λ ,$L^{\downarrow}atm(\lambda)$, $L^{\uparrow}atm(\lambda)$) are estimated, by the web atmospheric correction parameters calculator, at time of satellite overpass [30].

ε_0 is the surface emissivity which is estimated from the vegetation index (NDVI) [31]:

$$\varepsilon_0 = 1.0094 + 0.047 \times \ln(NDVI) \quad (5)$$

Spectral radiances $L_\lambda(T_0)$ reflected from the Earth surface can be deducted by inversion of Equation 4. After converting TIRS band data from DN to spectral radiance, we convert them to the top of atmosphere brightness temperature using the thermal constants provided in the metadata file:

$$T = \frac{K_2}{Ln\left(1 + \frac{K_1}{L_\lambda}\right)} \quad (6)$$

Where:

T Top of atmosphere brightness temperature (K)
L_λ TOA spectral radiance (Watts/(m^2 * srad * μm))
K_1 Band-specific thermal conversion constant from the metadata (K1_CONSTANT_BAND_x, where x is the thermal band number 10 or 11)
K_2 Band-specific thermal conversion was constant from the metadata (K2_CONSTANT_BAND_x, where x is the thermal band number 10 or 11).

Table 2. Band-specific thermal conversion constant from the metadata K1 and K2 values.

Thermal constant	Band 10	Band 11
K1	774.8853	480.8883
K2	1321.0789	1201.1442

TIRS bands were designed to allow the calculating surface temperature. For our analysis and calculation of LST, we used only bands 10 from the Thermal Infrared Sensor (TIRS) of the Landsat 8 satellite. According to Wang, since TIRS band 11 data from the Landsat 8 have considerable uncertainty, he also recommended using only TIRS band 10 data as a single spectral band for any LST estimation [32]. Finally, the land surface temperature is calculated as follows:

$$LST = \frac{T_b}{1+\left(\lambda * \frac{T_b}{\rho}\right) L_n \varepsilon} \quad (7)$$

Where:

T_b = At-satellite brightness temperature (in Kelvin)
ε = emissivity
λ =.wavelength of emitted radiance (11.5 μm)
$\rho = h \times c/\sigma$ ($1{,}438 \times 10^{-2}$ m K)
σ = Boltzmann constant ($1{,}38 \times 10^{-23}$ J K^{-1})
h = Planck's constant ($6{,}626 \times 10^{-34}$Js)
c = Velocity of light ($2{,}998 \times 10^{8}$ m sec^{-1})

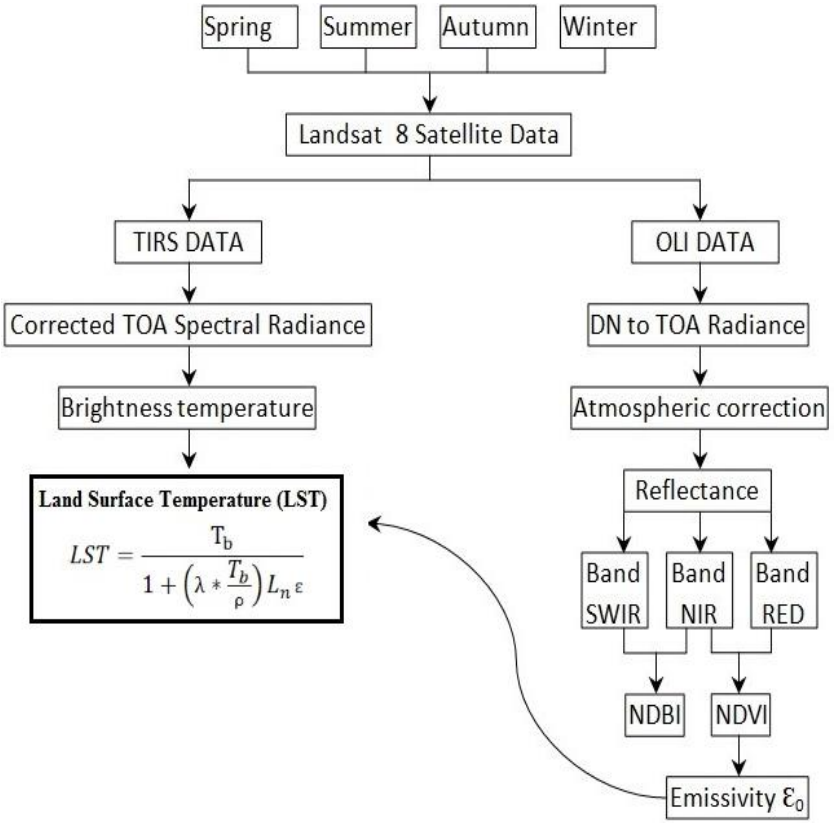

Figure 4. Flowchart of retrieving LST values from Landsat 8 image.

3. RESULTS AND DISCUSSION

Urbanization is one of the most influential forces that drive and affect climate warming. LST Maps created in this study have shown clearly the spatiotemporal changes in LST values over the sub-watershed of Oued Fekan area. The study aims to compare NDBI and NDVI as indicators of surface urban heat island by looking for the best correlation between both indicators with LST using Landsat 8 Imagery.

Table 3 summarizes the LST, NDVI and NDBI statistical data for the different four seasons. The results obtained from the study of Mean for LST, NDVI and NDBI profiles in section 2 indicate that both temperature and NDBI values change proportionally (see Fig. 5). Low values are recorded during February (respectively 18,524 °C and -0,017 for LST and NDBI values), while the high values appear in May and August (respectively 43,07 °C and 0,059 for LST and NDBI values). Otherwise, low values of NDVI are recorded for November and August (due to the low chlorophyllin activity) while the high values concern the month of February (0.321 of NDVI value), which decreases progressively until May.

Land cover types have different behaviour towards LST as well as NDVI and NDBI indices. Water bodies and vegetation show lower LST, whereas built up and bare soil region shows higher LST during daytime [33]. Despite only one land use unit such as vegetation, water body or impervious land, also create differences in LST (see sections 3.3 and 3.4 for more details) so that

urban areas, because of their impermeability land properties, are characterized by both high temperature and NDBI values. A low surface temperature often characterises contradictory, agricultural areas (non-urban areas).

Table 3. LST, NDVI and NDBI statistical data for four seasons.

Date	Minimum			Maximum			Mean			Standard Deviation		
	LST	NDVI	NDBI	LST	NDVI	NDBI	LST	NDVI	NDBI	LST	NDVI	NDBI
November 18th 2018	-1,8	-0,31	-0,41	26,66	0,83	0,38	20,122	0,169	0,014	2,091	0,088	0,059
February, 20th 2018	6,93	-0,27	-0,41	33,74	0,91	0,21	18,524	0,321	-0,017	3,246	0,127	0,083
May, 26th 2018	24,29	-0,21	-0,46	50,46	0,84	0,37	41,157	0,265	0,025	3,187	0,079	0,06
August 14th 2018	25,67	-0,17	-0,33	51,21	0,69	0,29	43,07	0,196	0,059	2,738	0,053	0,041

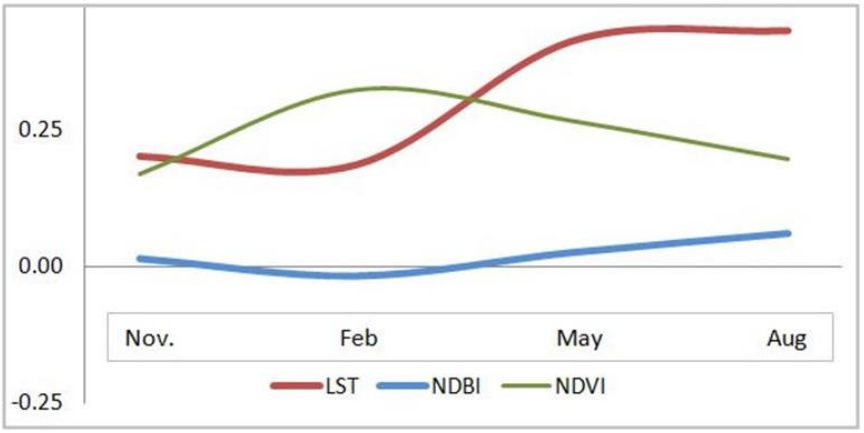

Figure 5. Mean representation for LST, NDVI and NDBI.

3.1. Spatiotemporal variation of LST

In order to study the behaviour of LST in our study area, the LST image was generated, as shown in figure 6. The area under study is characterized by recurrent drought, where the semi-arid climate is predominant. Two significant periods describe this area, dark and rainy period from November to March and another hot and dry, from April to October [18]. Winter (from December to February) is usually cold enough as the absolute minimum of the air temperature descends to -2 °C. Summer (from June to August) is usually hot and dry since the absolute maximum of the air temperature is equal to +50 °C. A hot drying wind from the South called "sirocco" accentuate the thermal maxima.

The remote sensing approach allowed measuring the LST of the entire study area, the interpretation of the spatial distribution of LST with the type of land use becomes possible. As it can be seen from Figure 6, especially fig 6.a, boundaries in south-eastern part are the coldest; on the other hand, the northwest part is warmer. It represents the Bouhanifia Mountains, an area known for its wealth of thermal water. It is found that the warmer area was also marked in the centre of the plain. Particularly where areas were filed agricultural and now marked as built-up areas. Temperature map shows that LST marks important values mainly at the built-up area and urban fallow land, which is going to be built up. During the winter season, the minimum and maximum of land surface temperature are 6.93 and 33.74 °C, respectively; for the summer season, the most basic marked value of LST is 25.67 °C while the maximum value is 51.21 °C.

An average of 43.06 °C during the hot summer season against an average of 18.524 °C during the cold winter, which clearly explains why this study area is classified as semi-arid in its type of climate.

The absence of a strong relationship between LST and UHI during the four seasons; especially in summer where bare land is predominant; returns to urban sprawl type exerted on the non-compact plain (except for major cities that are not metropolitan); otherwise it is discontinuous, scattered or diffuse and generally linear along the roads. This type of urban sprawl explains the homogeneity of LST marked in almost all the plain. Despite being an agricultural area, marked values are essential.

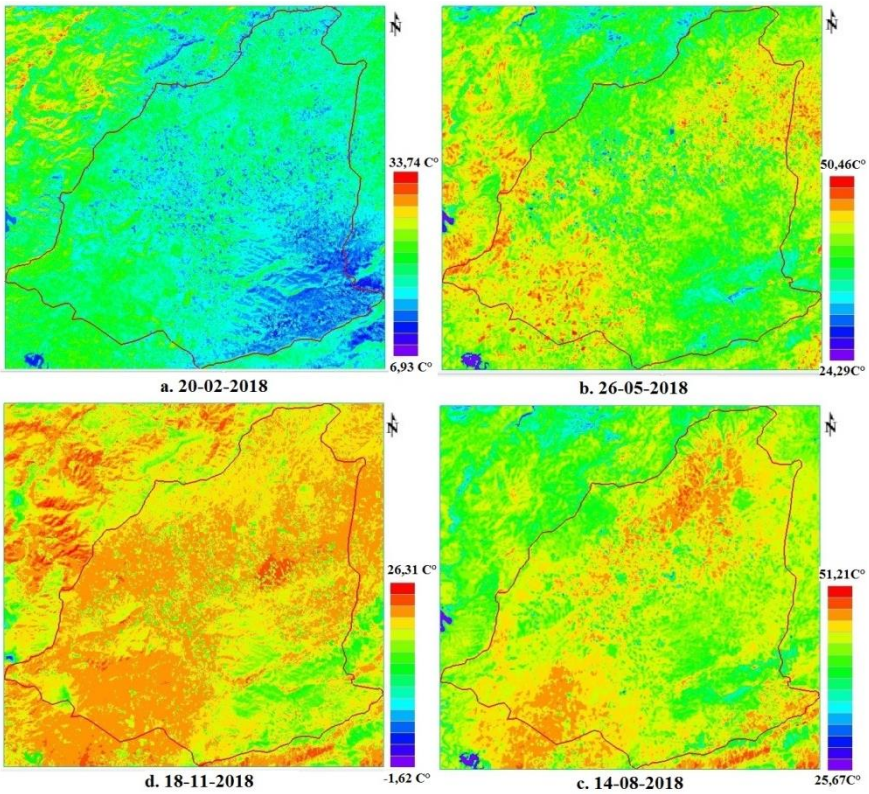

Figure 6. Spatial distribution of LST for four seasons in degrees Celsius (°C).

Validation of the spatial distribution of surface temperature and its relation to the type of land occupation, including UHI effects, is made as it can be seen in figure 7. The resulting LST class was located on the imagery. It was observed that Oued Fergoug show very low LST, also parcels with a high density of vegetation. The urban areas of Mascara city show LST higher than the vegetated areas and water-body but lower than the bare soil.

Urban areas of Mascara, Tighenif and Ghriss cities have marked a difference in the surface temperature higher than adjacent agricultural parcels of the plain about 2 to 3 °C in winter. This difference in LST changed along with the variation of season; these results involve studying the relationship between Normalized Difference Built Index and Land Surface Temperature and analyzing implications of urban growth on thermal characteristics.

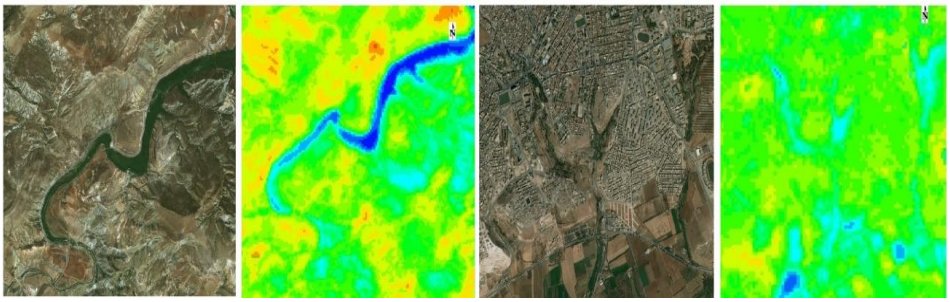

Figure 7. Visual interpretation of LST distribution using Reference Maplink

3.2. Spatiotemporal variation of NDVI and NDBI

Spatial representation of NDVI and NDBI distribution over the four seasons are shown respectively in figure 8 and figure 9. Firstly, relationships between NDVI and NDBI was analysed; a weak and negative correlation was marked between the two variables. An inverse relationship between NDVI and NDBI was marked. Height values of NDVI indicate vegetated areas; while height values of NDBI indicate built-up areas and barren land. Both indices were used to differentiate the land use/cover types of our study area. The most significant correlation occurred in summer. It suggests that NDVI can respond to NDBI change and reflect the evolution of the urban construction land (Figure 10).

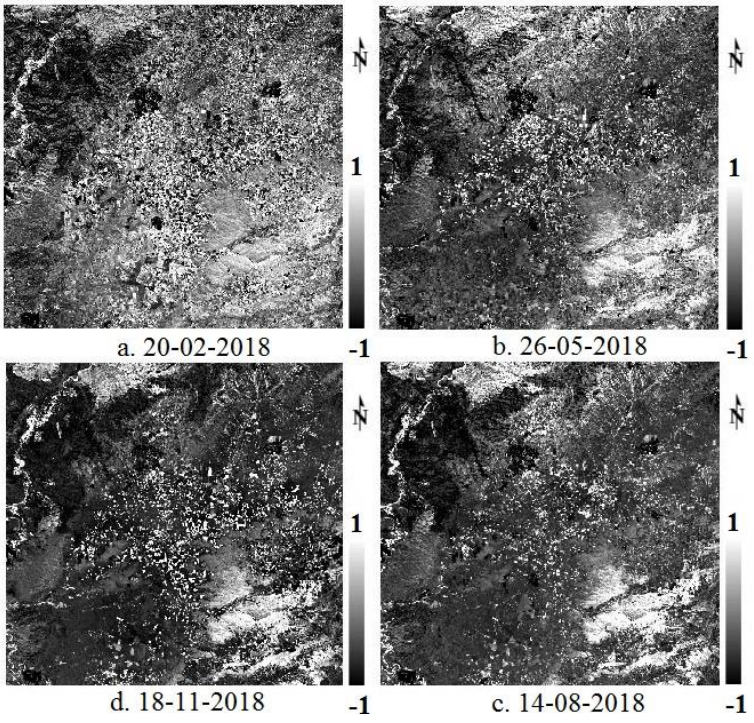

Figure 8. Spatial distribution of NDVI for four seasons

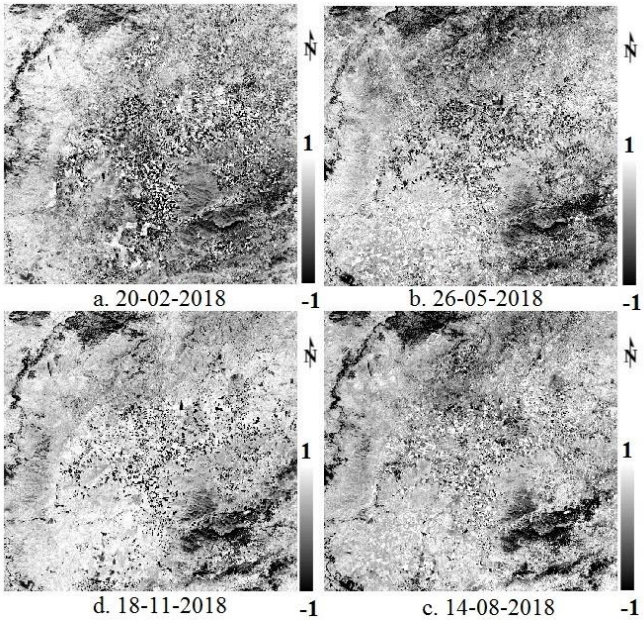

Figure 9. Spatial distribution of NDBI for four seasons

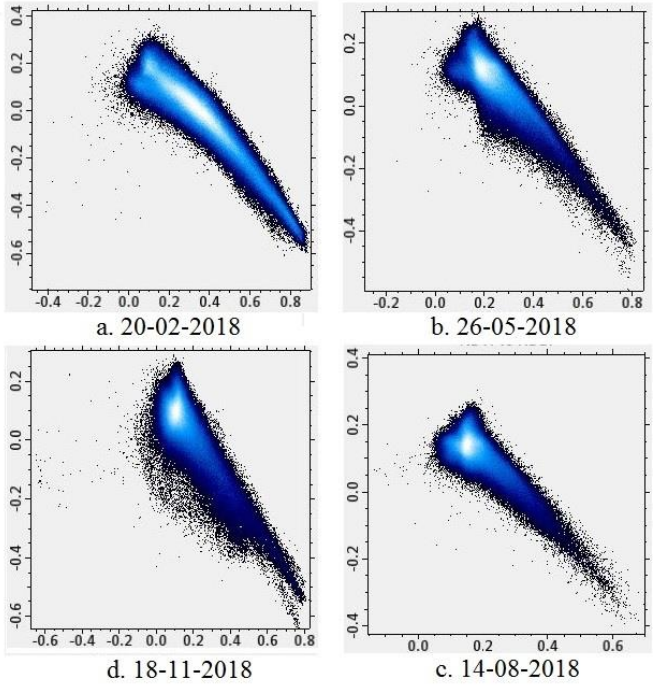

Figure 10. Scatter plots of NDVI (x-axes) and NDBI (y-axes) for four seasons

3.3. Relationships between the LST and NDVI

In order to study the relation of LST with the respective indices, scatter plots were obtained for LST/NDVI, LST/NDBI, as shown in Figure 11 – 12, respectively. Areas with high temperature generally tend to have lower NDVI values. This aspect has mainly corroborated from the analysis of the relationship between LST and NDVI. As shown in the LST images, the LST values of non-vegetated areas (dried river beds, barren land, built-up) are higher than those marked for areas of water bodies and vegetation, including agricultural land. The results obtained from the correlation between LST and NDVI showed non-linear behaviour between them. In urban regions, NDVI cannot explain LST due to more significant heterogeneity in land cover, especially in urban areas that include soil, buildings, vegetation and water. NDVI cannot well describe the LST of the study area since the trend of LST and NDVI relationship during seasons is different. Affected by the seasons, the relationship between NDVI and LST cannot achieve a stable level which indicates that the correlation between the two indices is influenced by season.

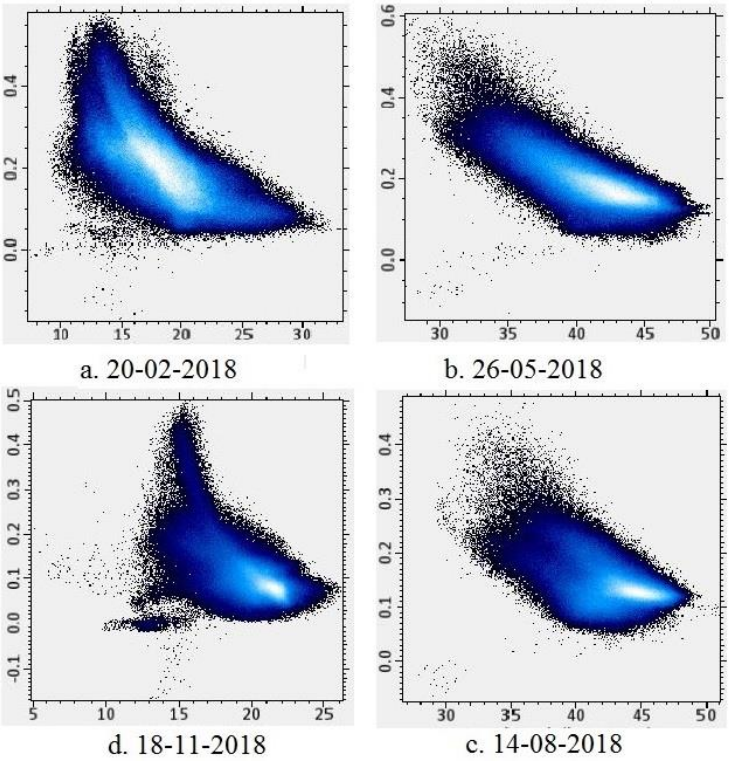

Figure 11. Scatter plots of LST (x-axes) and NDVI (y-axis) for four seasons

As shown by Figure 12, higher LST values are usually found in the areas of higher NDBI values because of the predominance of high-density urban areas, including commercial, industrial, and residential developments. In contrast, analysis of the above data shows that LST correlates closely with NDBI. There is a strong positive correlation between the values of both indices, indicating a direct relationship between them. As NDBI values increase LST values also

increase; generally in the same areas. Instead NDVI, NDBI can be used to study LST in the region containing different land covers.

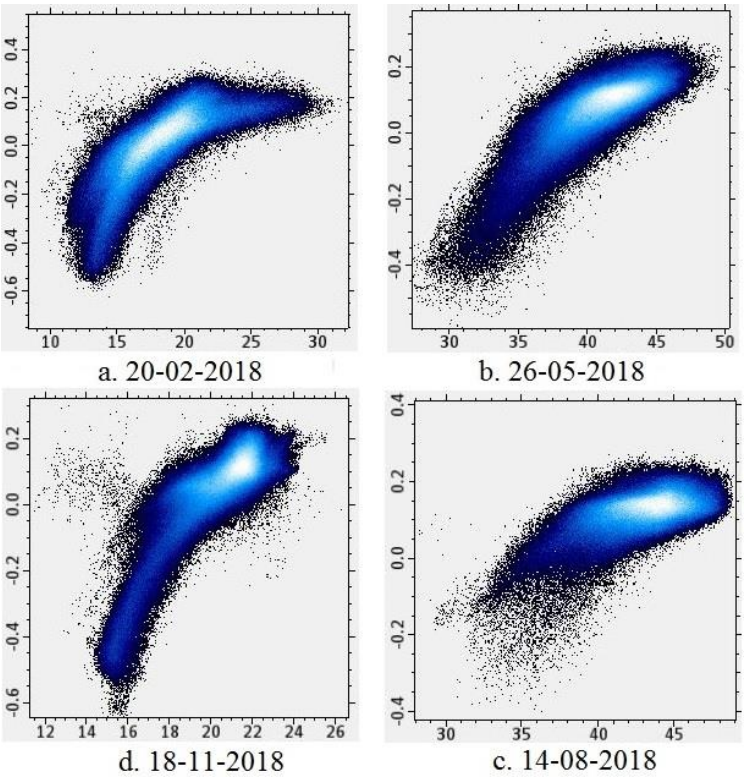

Figure 12. Scatter plots of LST (x-axes) and NDBI (y-axis) for four seasons.

3.5. A further investigation between LST, NDBI and NDVI

A deeper interpretation between the mean of LST, NDBI and NDVI was applied over all the heterogeneous area that encompasses the three cities of Mascara, Maoussa and Tighennif. Thus a large area of agricultural land showed a very strong positive relationship between the mean of LST and NDBI for all seasons (r^2> 0.86). The supported method to set the pace of NDBI/NDVI is explained in the following relation:

$$Pace_{NDBI} = (MAX_{NDBI} - MIN_{NDBI})/n$$

$$Pace_{NDVI} = (MAX_{NDVI} - MIN_{NDVI})/n$$

Where:

n = number of points retained; (Mostly we fixed n at 50 points).

The obtained results are presented in Fig. 13 and Fig. 14:

Contrariwise, the relationship between the mean of LST and NDVI was not accurate, in all graphs (Figure 13), we note that there is a stabilisation indicating a strong negative correlation between NDVI and LST(r2 of NDVI vs. LST ranges from 0.001 to 0.049). These inverse linear correlations begin when NDVI>0.2 for spring and summer. This same negative correlation starts

instead of when NDVI reaches the value of 0.18 for February and November. Results obtained show a negative correlation which varies by season; for values lower than the one mentioned before (NDVI<0.2 for May and August, NDVI<0.18 for February and November) including negative values which represent mainly non-vegetated area, urban surfaces and bare soil, no stable trend was identified. NDVI has an evident seasonal change which implies using this index is complicated to understand UHI.

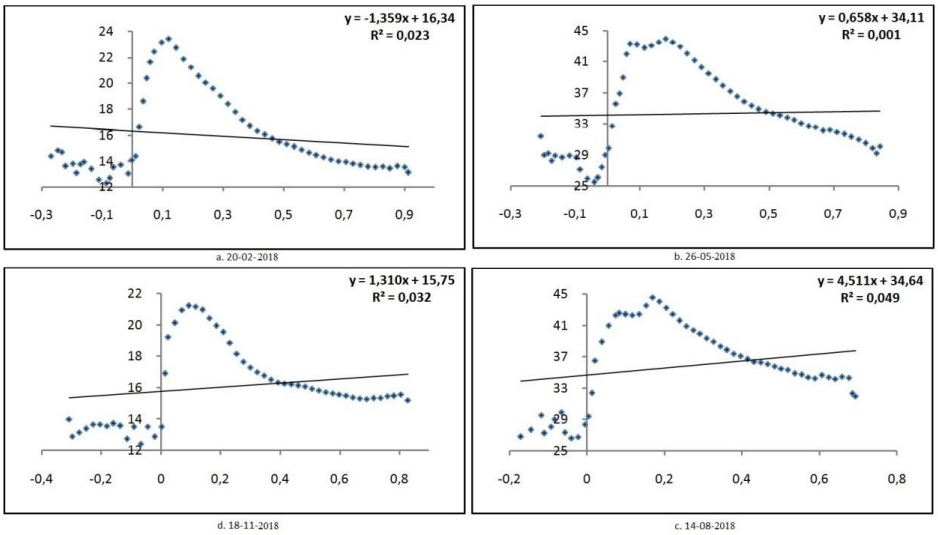

Figure 13. Relationship between NDVI and the mean of LST.

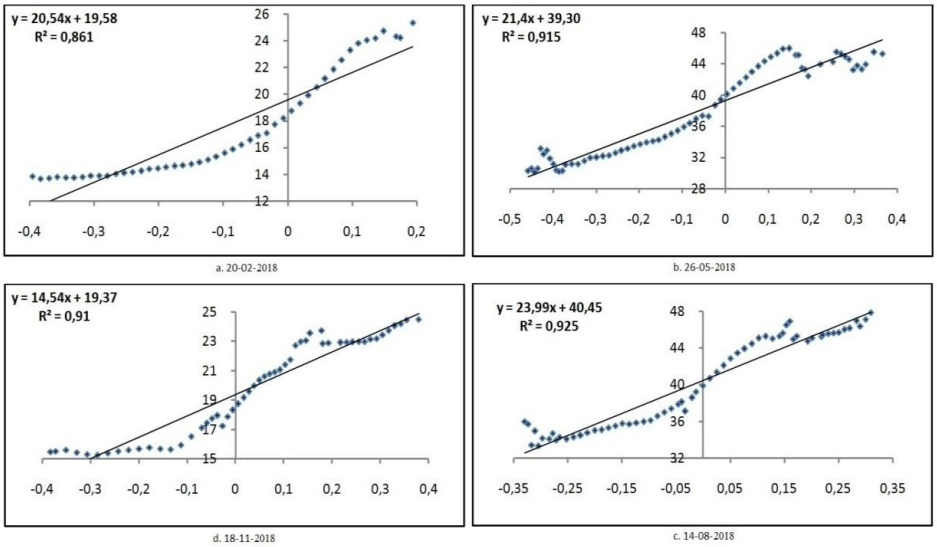

Figure 14. Relationship between NDBI and the mean of LST.

Conversely, as shown in figure 14, the co-linear correlation between NDBI and the mean of LST (r2 of NDBI vs. LST ranges from 0.861 to 0.925) was marked. LST is almost co-linear with air temperature as indicated by significant correlation value (0.861 for February, 0.915 for May, 0.925 for August and 0.91 for November 2018) at 0.02 level of significance. Its less variation with the season (not subject to seasonal effects) makes it an apparent index for future analysis of spatiotemporal UHI effects. The relationship between NDBI and LST was more stable comparing to NDVI and LST. NDBI can adequately describe the LST since they were positively correlated in four seasons (without seasonal effects.). The full index can be used as a supplemental indicator to the traditionally applied NDVI for further analysing seasonal changes in UHI effects.

3.6. Spatial dependence and correlation among NDBI, NDVI and LST from two profiles

To study a deeper Spatio-temporal distribution of LST, NDBI and NDVI, which is profiles of each index are drawn in two different areas. The first, located in Mascara city, covers buildings, roads, settlement and vegetation. While the second, located in the western part, covers water of Bouhanifia dam, sparse settlement and grassland that around it. Horizontal and vertical profiles have been made across the study area to represent the LULC wise LST (Figure 15). Profiles lines are shown in high-resolution Google Earth images acquired in 05/04/2018.

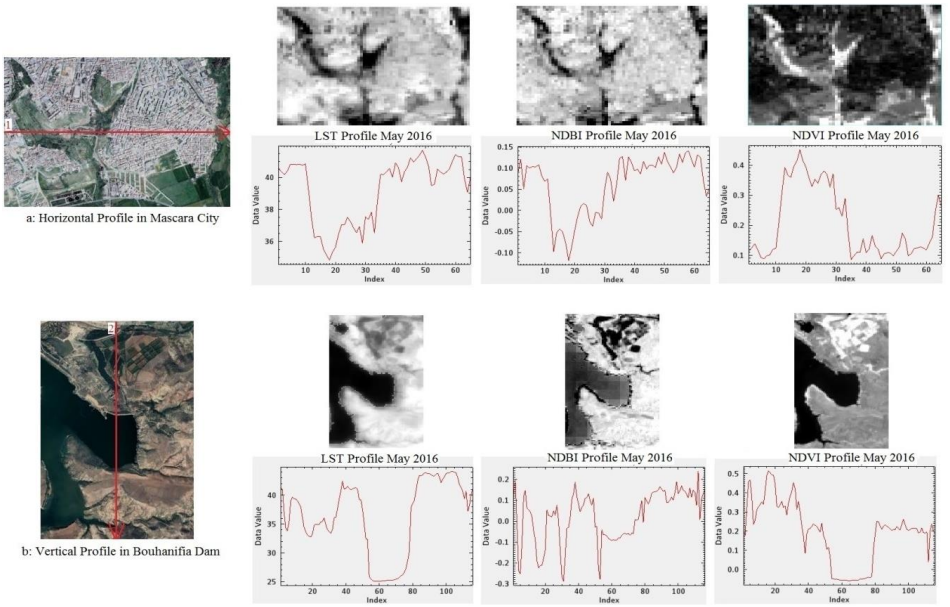

Figure 15. Selected LST, NDBI and NDVI Profiles.

By analysing obtained maps and profiles, it is identified that built-up areas like buildings, roads are warmer than vegetation-covered areas and grassland, but water bodies remain coolest of all. The urbanization process in sub-watershed of Oued Fekan had a significant impact on its thermal characteristics since the mean temperatures were higher in urban areas than in the surrounding suburban/rural areas. Heavily industrialized districts and built-up land, densely populated, are closely associated with high-temperature anomalies. Except in wetlands and waters where the NDVI profile shows a better correlation, both profiles of LST and NDBI varies in parallel with a strong correlation. All three indices (LST, NDBI and NDVI) used in our study, can

describe, in a qualitative manner, the spatial distribution and temporal variation in the plain thermal environment.

Extracting LST from thermal remote sensing data is useful for studying other subjects such as evapotranspiration. Results obtained showed that industrialized districts and built-up land, densely populated, are closely associated with high-temperature anomalies. We recommend controlling the urbanization exercised in Ghriss plain, avoiding compacted urban sprawl, with thoughtful planning of the distribution of industry, which will mitigate the UHI effect for a healthy urban environment and sustainable development.

4. CONCLUSION

Analysing the spatial distribution of LST is a factor key in the different studies such as urban heat island studies, climate change studies and also evapotranspiration studies. This paper focused on the investigation of the relationship among the LST, NDVI and NDBI in the sub-watershed of Oued Fekan of approximately 1190 km2 surrounding Mascara city in the north-west of Algeria. The relationship equations have been derived between LST and NDBI values for four different seasons represented, respectively by October, February, May and August. Then, analyses were based on the interpretation of remote sensing data of Landsat-8 OLI-TIRS imagery. Results indicate that different types of land use/cover and urban sprawl exerted in the plain have an essential impact on land surface temperature. However, the strong linear relationship between the LST and NDBI for all seasons suggests that urban areas have the most impact on LST distributions, i.e. urban areas of Mascara, Tighenif and Ghriss have marked a higher difference in the surface temperature than near agricultural parcels of about 2 to 3 °C in winter, while it differs from one season to another.

Detailed analysis shows that this variation in the distribution of LST can be better accounted for by NDBI than by the commonly used NDVI since the correlation of LST with NDBI was found better than NDVI, which implies that NDBI is an accurate indicator of surface heat island effects. This finding suggests that some measures (e.g., increasing forest and garden lands, controlling the population density in Ghriss plain, thoughtful planning of the distribution of industry), could be taken to mitigate the UHI effect for a healthy urban environment and sustainable development. Availability of remote sensing data covering the overall North-west of Algeria allows in further studies to project the contemporary approach on the metropolitan coastal town of Oran with different climatic conditions and different land use/cover types.

Acknowledgements

The authors would like to thank in advance the anonymous reviewers who will help to improve this paper. The authors wish to thank the U.S. Geological Survey (USGS) and the Earth Resources Observation and Science (EROS) Center for the availability of Landsat Products, as well as the USGS EROS User Services for their collaboration and their valuable answers to our questions.

REFERENCES

[1] Jing, J. & Tian, G. (2010). Analysis of the impact of Land use/Land cover change on Land Surface Temperature with Remote Sensing. Procedia Environ. Sci.2,571-575. https://doi.org/10.1016/j.proenv.2010.10.062

[2] Zhao-LiangLi& Bo-Hui Tang & Hua Wu & Hua zhong Ren &Guangjian Yan & Zheng ming Wan & Isabel F.Trigo José &A.Sobrino. (2013). Satellite-derived land surface temperature: Current status and perspectives. Remote Sensing of Environment, Vol. 131, no.15, pp. 14-37.DOI:10.1016/j.rse.2012.12.008

[3] Oke, T.R. (1973). City size and the urban heat island.Atmos. Environ. 7:769–779, http://dx. DOI.org/10.1016/0004-6981(73)90140-6.

[4] Dousset, B.&Gourmelon, F. (2003).Satellitemulti-sensor data analysis of urban surface temperatures and land cover. ISPRS J. Photogramm. Remote Sens. 58:43–54. http://dx.DOI.org/10.1016/S0924-2716(03)00016-9.

[5] Sun, Q.& Tan, J.& Xu, Y. (2010). An ERDAS image processing method for retrieving LST and describing urban heat evolution: a case study in the Pearl River Delta Region in South China. Environ. Earth Sci. 59 (5), 1047–1055.https://DOI.org/10.1007/s12665-009-0096-3

[6] Liu, L.& Zhang, Y.(2011). Urban Heat Island analysis using the Landsat TM data and ASTER data: a case study in Hong Kong. Remote Sens. 3:1535–1552. DOI: 10.3390/rs3071535

[7] Lu, Y.& Feng, P.& Shen, C.& Sun, J. (2009).Urban heat island in summer of Nanjing based on TM data. Urban Remote Sensing Joint Event, Shanghai, China: pp. 1–5.DOI.org/10.1109/URS.2009.5137628.

[8] Buyantuyev, A.& Wu, J. (2010).Urban heat islands and landscape heterogeneity: linking spatiotemporal variations in surface temperatures to land-cover and socioeconomic patterns. Landsc. Ecol. 25:17–33. DOI.org/10.1007/s10980-009-9402-4.

[9] Weng, Q. (2003). Fractal analysis of satellite-detected urban heat island effect.Photogramm.Eng. Remote. Sens. 69, 555–566.https://doi.org/10.14358/PERS.69.5.555.

[10] Weng, Q.& Lu, D.&Schubring, J.(2004).Estimation of land surface temperature e vegetation abundance relationship for urban heat island studies.Remote Sens. Environ. 89: 467–483.DOI.org/10.1016/j.rse.2003.11.005.

[11] Balling, R.C.&Brazel, S.W. (1988). High resolution surface temperature pattern in a complex urban terrain. Photogramm. Eng. Remote. Sens. 54 (9), 1289–1293.

[12] Sobrino, J.A.&Coll, C.&Caselles, V. (1991). Atmospheric correction for land surface temperature using NOAA-11 AVHRR channels 4 and 5. Remote Sens. Environ. 38 (1):19–34.DOI.org/10.1016/0034-4257(91)90069-I.

[13] Streutker, D.R. (2002). A remote sensing study of the urban heat island ofHouston, Texas.Int. J. Remote Sens. 23 (13):2595–2608. DOI.org/10.1080/01431160110115023.

[14] Streutker, D.R. (2003). Satellite-measured growth of the urban heat island of Houston, Texas.Remote Sens. Environ. 85:282–289.DOI.org/10.1016/S0034-4257(03)00007-5.

[15] Weng, Q.& Lu, D.&Schubring, J. (2004). Estimation of land surface temperature e vegetation abundance relationship for urban heat island studies. Remote Sens. Environ. 89: 467–483. DOI.org/10.1016/j.rse.2003.11.005.

[16] Fu, P.&Weng, Q. (2016).Consistent land surface temperature data generation from irregularly spaced Landsat imagery.Remote Sens. Environ. 184:175–187, 2016.DOI.org/10.1016/j.rse.06.019.

[17] Hu, L.&Brunsell, N.A. (2013).The impact of temporal aggregation of land surface temperature data for surface urban heat island (SUHI) monitoring.Remote Sens. Environ. 134:162–174.DOI.org/10.1016/j.rse.2013.02.022.

[18] Nehal, L.&Hamimed, A.&Khaldi, A.&Souidi, Z.&Zaagane, M.(2017).Evapotranspiration and Surface Energy Fluxes Estimation Using the Landsat-7 Enhanced Thematic Mapper Plus Image over a Semiarid Agrosystem in the North-West of Algeria. RevistaBrasileira de Meteorologia, v. 32, n. 4, 691-702. DOI:http://dx.DOI.org/10.1590/0102-7786324016

[19] Hua Li, Qinhuo Liu, "Comparison of NDBI and NDVI as indicators of surface urban heat island effect in MODIS imagery," Proc. SPIE 7285, International Conference on Earth Observation Data Processing and Analysis (ICEODPA), 728503 (29 December 2008); https://doi.org/10.1117/12.815679

[20] Mushore, T.D., Mutanga, O., Odindi, J., & Dube, T. (2016). Assessing the potential of integrated Landsat 8 thermal bands, with the traditional reflective bands and derived vegetation indices in classifying urban landscapes. Geocarto International, 1–14. doi:10.1080/ 10106049.2016.1188168

[21] Ma, Q., Wu, J., & He, C. (2016). A hierarchical analysis of the relationship between urban impervious surfaces and land surface temperatures: Spatial scale dependence, temporal variations, and bioclimatic modulation. Landscape Ecology, 31, 1139–1153.

[22] Tran., D.X., Pla, F., Carmona, P.L., Myint, S.W., Caetano, M., & Kieua, P.V. (2017). Characterizing the relationship between land use land cover change and land surface temperature. ISPRS Journal of Photogrammetry and Remote Sensing, 124, 119–132.

[23] Deilami, K., & Kamruzzaman, M. (2017). Modeling the urban heat island effect of smart growth policy scenarios in Brisbane. Land Use Policy, 64, 38–55.

[24] Estoque, R.C., Murayama, Y., & Myint, S.W. (2017). Effects of landscape composition and pattern on land surface temperature: An urban heat island study in the megacities of southeast Asia. Science of the Total Environment, 577, 349–359.

[25] Subhanil Guha, Himanshu Govil, Anindita Dey & Neetu Gill (2018) Analytical study of land surface temperature with NDVI and NDBI using Landsat 8 OLI and TIRS data in Florence and Naples city, Italy, European Journal of Remote Sensing, 51:1, 667-678, DOI:10.1080/22797254.2018.1474494

[26] Bekkoussa, S.&Bekkoussa, B.&Taupin, J. D.&Patris, N.&Meddi, M. (2018).Groundwater hydro chemical characterization and quality assessment in the Ghriss Plain basin, northwest Algeria. Journal of Water Supply: Research and Technology-Aqua, jws2018013.DOI: 10.2166/aqua.2018.013.

[27] Berk, A.; Confortı, P.; Hawes, F.; Perkıns, T.; Guıang, C.; Acharya, P. (2016). Next Generation MODTRAN for Improved Atmospheric Correction of Spectral Imagery. Spectral Sciences, Inc. Burlington United States.

[28] Hamadouche, M. A.&Mederbal, K.&Khaldi, A.&Kouri, L.&Fikir, Y&Anteur, D. (2017). GIS Based Remote Sensing Data to Monitor Biodiversity in the Cultural Parks of Ahaggar and TassilNajjer (Southeast of Algeria). Journal of Applied Environmental and Biological Sciences. ISSN: 2090-4274.

[29] Zha, Y. & Gao, J. & NiI, S. (2003). Use of normalized difference built-up index in automatically mapping urban areas from TM imagery. Int. J. Remote Sens. 24 (3):583–594. DOI.org/10.1080/01431160304987.

[30] Barsi, J.A.& Barker, J.L.& Schott, J.R. (2003).An Atmospheric Correction Parameter Calculator for a Single Thermal Band Earth-Sensing Instrument.J. Proc. IEEE. Int. v. 5,p. 3014-3016.

[31] Van de griend, A.A. & OWE, M. (1993). On the relationship between thermal emissivity and the normalized difference vegetation index for natural surfaces. Int. J. Remote. Sens, v. 14,p. 1119-1131. DOI: 10.1080/01431169308904400.

[32] Wang, F.& Qin, Z.& Song, C.& Tu, L.&Karnieli, A.& Zhao, S. (2015). An improved mono-window algorithm for land surface temperature retrieval from Landsat 8 thermal infrared sensor data.Remote Sens. 7:4268–4289. https://DOI.org/10.3390/rs70404268

[33] Amiri, R., Weng, Q., Ali mohammadi, A., &Alavipanah, S. K. (2009).Spatial-temporal dynamics of land surface temperature in relation to fractional vegetation cover and land use/cover in the Tabriz urban area, Iran.Remote Sensing of Environment, 113, 2606–2617.